water

MDPI

Article

Experimental Investigations on Influence of Fracture Networks on Overland Flow and Water Infiltration in Soil

Jin You [1,2,*], Shuqian Wang [1,2] and Dan Xu [1,2,*]

[1] School of Water Conservancy and Hydroelectric Power, Hebei University of Engineering, Handan 056021, China
[2] Hebei Key Laboratory of Intelligent Water Conservancy, Hebei University of Engineering, Handan 056038, China
* Correspondence: youj0226@163.com (J.Y.); xudan930328@163.com (D.X.); Tel.: +86-130-2193-0226 (J.Y.); +86-182-3205-8336 (D.X.)

Abstract: Soil preferential flow is an essential process that affects the movement and relocation of soil water and solutes. This study was conducted on cropland in an arid and semi-arid area in Zhongning County, Ningxia. According to the different cracks, rain intensity, rainfall duration, and slope, there were three groups, and 17 dye tracer experiments were conducted in the field. We quantified the characteristics of soil preferential flow by investigating and analyzing the infiltration depth, dyeing area, saturation, runoff coefficient, and rainfall infiltration coefficient using the dye tracer method. The results showed that increasing the rainfall or irrigation intensity could promote the activation of the fracture channel as the preferential flow channel, which is advantageous to the preferential flow formation. The fractures dominated the formation of the preferential flow. The fractures slowed the formation of runoff, reduced the velocity of slope flow, reduced the flow of the slope, and increased the amount of soil water infiltration. These results have theoretical and practical significance for understanding soil water transportation, especially for agricultural irrigation management and improving cropland water use efficiency in arid and semi-arid areas.

Keywords: preferential flow; dye tracer test; soil matrix; soil fracture; water infiltration

check for updates

Citation: You, J.; Wang, S.; Xu, D. Experimental Investigations on Influence of Fracture Networks on Overland Flow and Water Infiltration in Soil. *Water* **2022**, *14*, 3483. https://doi.org/10.3390/w14213483

Academic Editors: George Kargas, Petros Kerkides and Paraskevi Londra

Received: 22 September 2022
Accepted: 28 October 2022
Published: 31 October 2022

Publisher's Note: MDPI stays neutral with regard to jurisdictional claims in published maps and institutional affiliations.

Copyright: © 2022 by the authors. Licensee MDPI, Basel, Switzerland. This article is an open access article distributed under the terms and conditions of the Creative Commons Attribution (CC BY) license (https://creativecommons.org/licenses/by/4.0/).

1. Introduction

Dry soil shrinkage cracks in farmland play an important role in the preferential flow of soil and the migration of solute and environmental pollutants, causing widespread concern to researchers in soil science, agriculture, engineering geology, and environmental protection [1,2]. The generation and closure of fractures are accompanied by shrinkage and expansion in the soil. They are affected by physically, chemically, and biologically intrinsic properties such as soil water content, soil clay minerals, and soil organic matter under external environmental conditions, such as drying–wetting alternation, crop growth, tillage, etc. [3]. Soil is often subject to drying–wetting alternation conditions due to precipitation, irrigation, and evapotranspiration. The intensity of dry and wet alternation significantly affects soil shrinkage [4]. With increases in dry and wet alternation times, the area density of the fissure shows a downward trend [5]. Soil contractility tends to decrease, and the original fractures will diffuse to the surroundings again when the desiccant is dehumidified. The width of the cracks decreases correspondingly, and the quantity shows an increasing trend [6]. Vogel et al. [7] used topology theory to describe networks of soil fractures and applied topological concepts and methods to establish parameters such as crack area, length, and Euler's densities to characterize them.

Fractures generated during soil shrinkage in farmland can be used as preferential flow channels, allowing part of the soil water to bypass the soil matrix and rapidly infiltrate along the fissures, which is widely recognized as a common phenomenon in hydrology [8–10]. Fractures can serve as a preferential flow path during irrigation or rainfall, accelerating

water infiltration, reducing the use efficiency of water and fertilizer, and increasing the risk of groundwater pollution [11,12]. At the same time, they are one of the inducing factors of geological disasters, such as debris flow, landslides, collapses, and soil erosion. When rainwater enters the fractured soil from the slope surface, it flows in the fractured network and infiltrates the soil matrix. Compared with nonfractured soil, the presence of fractures increases the infiltration capacity and the lateral flow of soil water, ultimately affecting the slope's hydrology [13–15]. The occurrence of dry-shrinkage cracking not only affects the water movement in the soil but also affects the surface runoff dynamic parameters due to factors such as the slope flow rate, the single-width flow rate, and Reynolds number reduction [16].

The dye tracer technique is an experimental technique that reveals the soil preferential flow phenomenon using a dye that penetrates the soil with water flow infiltration. Due to its distinctive color, low cost, obvious color difference compared with the soil matrix, and short experiment time, the dye tracer technique has become the most common method of studying preferential flow [17–19]. The dye solution is usually sprayed on the soil surface using simulated rainfall. After the infiltration is complete, the direct distribution of the soil preferential flow path can be obtained by excavating the soil profile (horizontal profile or vertical profile) to provide a basis to further analyze the migration patterns of the soil water and solute. Flury [20,21] pointed out that the ideal dye tracer for soil flow movement is characterized by distinct color recognition, high solubility, and nontoxicity or low toxicity. In recent years, a large number of studies [22] have shown that brilliant blue (FCF, color index: 42090) has the above characteristics and is an ideal dye. However, it should be noted that the adsorption of the bright blue molecules by soil cosmids results in the lasing range of the bright blue dye significantly lagging behind the actual migration range of the infiltration wetting front [23]. As a result, I^- ions are not completely adsorbed by the soil clay [11] and are consistent with the migratory characteristics of soil infiltration and the wetting front. Because brilliant blue also possesses qualities such as high solubility and low toxicity, it is easily recognizable due to its blue-purple color reaction, which is especially suitable for preferential flow tracing in cohesive soils. More and more studies [24,25] use a high concentration of (15~30 g/L) I^- solution for dye tracer experiments. Flury et al. [26] studied differences in macropore flow in various soil types using bright blue dye. Sheng et al. [19] used iodine–starch dye to study the effect of macropores on water and solute migration and distribution. Wang et al. [27] used iodine–starch dye and bright blue tracer to study water migration in heterogeneous soils.

In recent years, due to a series of soil erosion and environmental pollution problems caused by the irrational use of land resources, more and more attention has been paid to the soil solute preferential migration phenomenon. Researchers have conducted a lot of research on the definition [28], type [29], degree [30], features [31–33], scale, methods [34,35], and models [36,37] of preferential flow, and the results have significantly guided the improvement of preferential flow theory and observation technology. However, most previous studies were conducted indoors, and the soil matrix area and soil cracks were separated from each other. In practice, there are many differences between farmland soil and cracks and laboratory conditions, and there is an interactive relationship between the preferential migration of solutes in soil matrix zones and crack zones.

In this paper, 17 groups of field experiments were carried out by adjusting soil cracks, rainfall intensity, rainfall duration, and soil slopes. The soil matrix area and the fractured area were studied as a whole. The movement features of soil water in the surface layer, matrix area, and crack of farmland were analyzed based on the infiltration depth, dyed area, the contribution of preferential flow infiltration to total infiltration, and other parameters, thus revealing the mechanisms of farmland runoff and solute movement under the action of soil desiccation crack. The research results are of great significance for the in-depth knowledge of water movement and solute movement features in farmland, guiding agricultural irrigation and improving agricultural water use efficiency.

2. Materials and Methods

2.1. Experiment Sites

The experiment was carried out in the Yellow River irrigation area of Zhongning County, Ningxia (105.67° E, 37.48° N). Zhongning County is located in the midwest of the Ningxia Hui Autonomous Region, in the transition zone between Inner Mongolia Plateau and Loess Plateau, and in the north temperate monsoon climate zone, with an average annual temperature of 9.5 °C, average annual precipitation of 202.1 mm, with the precipitation from June to August accounting for 61% of the annual precipitation; the annual evaporation of 1947.1 mm is 9.6 times of the average annual precipitation. The field capacity (mass) is 23.82%, the average mass fraction of soil organic matter is 14.47 g/kg, and the pH value is 7.58. The soil in the experimental area is clay, and the physical properties are shown in Table 1.

Table 1. Physical soil properties in the experiment area.

Soil Depth/cm	Particle Size Distribution/%			Density/g·cm^{-3}	Porosity/%
	>50 μm	2~50 μm	<2 μm		
0~10	3.7	51.0	45.5	1.4253	45.2
>10~20	4.6	52.5	45.4	1.5445	45.0
>20~30	4.5	51.6	45.3	1.6876	44.8
>30~50	4.8	50.4	45.6	1.6424	44.3

2.2. Dye Tracer Experiments

2.2.1. Experiments on Dry Shrinkage Cracks in the Soil

The experiments were divided into 7 treatment groups according to different amounts of infiltration water, S1-1 to S1-7, as per Table 2. Each experiment area was 100 cm long and 100 cm wide, as shown in Figure 1. Before the experiment, the experiment area was fully saturated. According to the soil density of the experiment area, the fractures appearing during the evaporation and cracking processes of the S1-3 and S1-6 groups were landfilled. Three days later, a dye tracer experiment was carried out. The dye was selected to be a bright blue solution of 4 g/L. After the solution had completely penetrated the surface, the experiment area was covered with a plastic plate to avoid evaporation. After 14 h of infiltration, profiles were excavated layer by layer in the experiment area, and vertical profiles were excavated layer by layer at intervals of 5 cm in the axial direction and photographed for recording. After taking photographs, soil samples were collected from the stained and unstained regions to measure soil water content distributions. More than fifty soil samples were collected in the stained and unstained regions at depths of 0, 0.10, 0.20, 0.30, 0.40, 0.50, 0.60, 0.70, and 0.80 m.

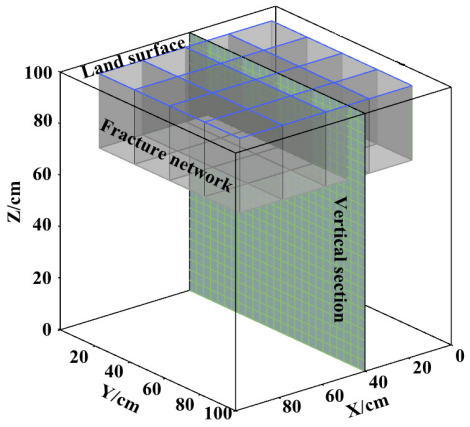

Figure 1. Diagram of S1 experimental setup.

Table 2. Experimental conditions of the plots.

Experiment Label	Precipitation Intensity/mm·h^{-1}	Duration of Precipitation/min	Volume of Water Infiltration/L	Existence of Cracks
S1-1			10	existent
S1-2			10	existent
S1-3			10	inexistent
S1-4			20	existent
S1-5			20	existent
S1-6			20	inexistent
S1-7			30	existent
S2-1	20	20	6.67	existent
S2-2	20	60	20	existent
S2-3	50	20	16.67	existent
S2-4	50	50	41.67	existent
S3-1	30	60	30	existent
S3-2	30	60	30	existent
S3-3	30	60	30	inexistent
S3-4	50	30	25	existent
S3-5	50	30	25	existent
S3-6	50	30	25	inexistent

2.2.2. Experiments in Artificial Crack Networks

The experiment was divided into four groups, S2-1 to S2-4, according to the different rainfall intensities and rainfall durations, as shown in Figure 2. Each experiment area was 100 cm long and 100 cm wide. An electric drill was used to punch the steel plate to extrude it into the soil at a thickness of 0.5 cm, forming a rectangular network of artificial soil fissures. The depth of each crack was 30 cm, and the length was 90 cm, a total of ten, as shown above. Before the experiment, the initial water content of the soil was measured by excavating the working profile (parallel to the Z-Y plane) on the side of the experiment area. When the experiment started, potassium iodide reagent (20 g/L) was added to the simulated rainfall source, and the experiment was carried out according to Table 2. Due to the intense evaporation in the research area, to ensure the water balance, after the tracer solution completely penetrated the earth's surface, we covered the experiment area with a tarpaulin to prevent evaporation. Finally, the vertical profile was excavated layer by layer every 5 cm along the *X*-axis of the experiment area, and spray starch solution was added to each layer. Sodium hypochlorite was added to the solution to accelerate the complete oxidation of iodide to iodine. The iodine reacted with the starch in a molecular state and permeated into the region where water passes by. As there was iodine, the iodine reacted with starch and turned blue. For regions where water did not pass, the color of the soil did not change. In this way, the flowing region and nonflowing region were confirmed. We then photographed the experiment profile and measured the soil moisture content. Soil samples were collected as described above.

2.2.3. Experiments in Artificial Crack Networks with Slope (10°)

The experiment was divided into six groups, S3-1 to S3-6, according to the different rainfall intensities and rainfall durations, as shown in Figure 3. Each experiment area was 100 cm long and 100 cm wide. We removed the surface floats and formed a sloped surface with a 10° angle to the horizontal. An electric drill was used to punch the steel plate to extrude it into the soil at a thickness of 0.5 cm, forming a rectangular network of artificial soil fissures. The depth of each crack was 30 cm, and the length was 80 cm, a total of ten, as shown above. Before the experiment, the initial water content of the soil was measured by excavating the working section (parallel to the Z-Y plane) on the side of the experiment area. When the experiment started, potassium iodide reagent (20 g/L) was added to the simulated rainfall source, and the experiment was carried out according to

Table 2. The time of surface runoff generation was recorded when the amount of water in the gauge increased by 100 mL. After the tracer solution completely penetrated the earth's surface, we covered the experiment area with a tarpaulin to prevent evaporation. Finally, the vertical profile was excavated layer by layer every 10 cm along the *X*-axis of the experiment area. For the tracer experiments, Fe^{3+} was used as a mild oxidizer for I^-, which does bleach the complex color of the formed starch–iodide. In addition, the effect of dissolving starch in the I^- solution was better than applying starch powder directly to the soil profile, avoiding a wetting process in the starch layer caused by the I^- solution in the soil. The indication solution consisted of 50 g/L of starch and 0.05 M of iron (III) nitrate ($Fe(NO_3)_3$). The indication solution was added with a pressurized sprayer that released a continuous and fine mist made up of an indication solution. The indication solution was sprayed on the surface as uniformly as possible with long, slow strokes. After spraying, it took about 10 min for a dark blue-violet color to develop in the flow zone as a result of the iron (III) nitrate oxidizer. We photographed the experiment section and measured the soil moisture content. The soil samples were collected as described above.

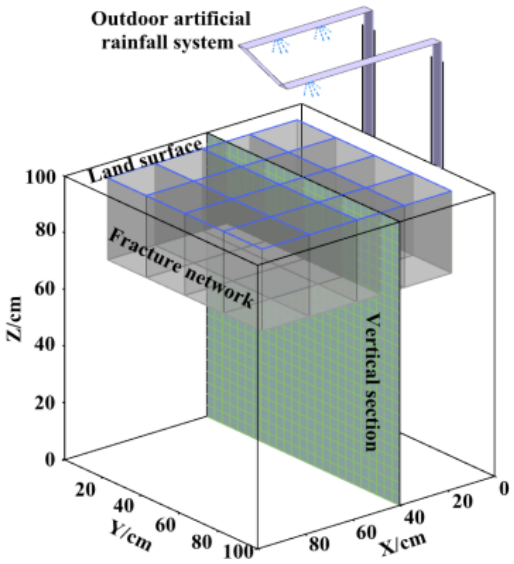

Figure 2. Diagram of S2 experimental setup.

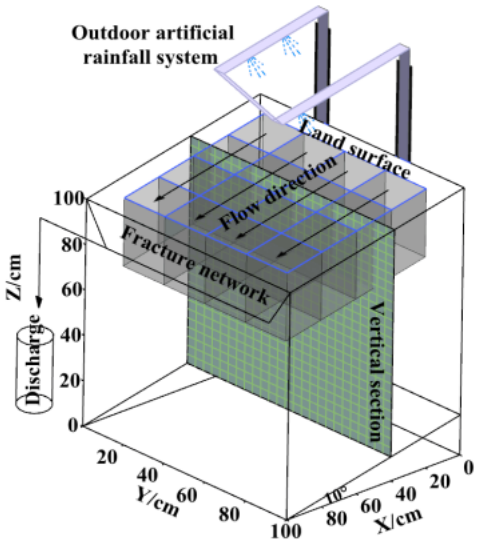

Figure 3. Diagram of S3 experimental set-up.

2.3. Image and Data Processing

To produce binary images that could then be analyzed quantitatively, an analysis of the images taken in the field was performed in two steps, as shown in Figure 4. Step 1 consisted of correcting for lighting and geometric distortions. The most important sources of variability in soil images are usually caused by uneven illumination, geometric distortion, and the condition of the surface [38,39]. These problems were minimized by fixing the environmental conditions and carefully preparing the soil face by hand prior to the acquisition of each image. Meanwhile, a sunshade and high-pixel camera were used when taking photos. In step 2, the modified image was converted to the BMP format in the 256-color RGB image pattern. Each pixel was analyzed to define whether it was dyed or not, based on threshold criteria for RGB reflectance values. Dyed pixels were defined as black and non-dyed pixels were defined as white [40]. We used the output data to calculate the following parameters to quantify the degree of preferential flow. To quantify the variability of soil water flow, the concept of actual penetration depth (H_a) was used [41]. To direct and quantitative the description of the vertical profile, movement trajectory (H_b) was used [42].

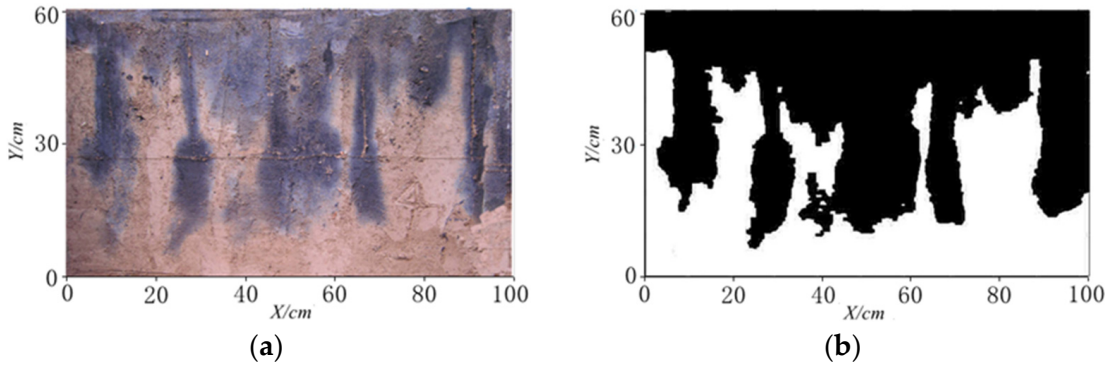

Figure 4. (**a**) The original image after correcting for lighting and geometric distortion; (**b**) a binary image after applying the dye detection algorithm.

Calculate the preferential flow parameters and quantify the preferential flow characteristics based on the binary data from image processing. The variability of soil moisture flow is quantified by the actual infiltration depth (*ID*), the movement track of the vertical profile is quantified by the dyed area (*DC*), and the infiltration uniformity S2 is used to indicate whether the soil moisture infiltrates to a uniform depth in the cracked area and matrix area.

The dyed area (*DC*) refers to the percentage of dyed area to the profile area and is calculated as follows:

$$DC = H_a(z) = \frac{\sum_{i=1}^{n} a(x_i, y_i, z)}{xy} \quad (1)$$

In the formula, when the cube pixels of coordinate a(x_i, y_i, z_i) are dyed, define a(x_i, y_i, z_i) = 1. If they are not dyed, define a(x_i, y_i, z_i) = 0, and xy is the total number of pixels in the profile.

The actual infiltration depth (*ID*) refers to the maximum area reached by the infiltration of soil water in the test region and is calculated as follows:

$$ID = H_a(x, y) = \sum_{i=1}^{n} a(x, y, z_i)\Delta h \quad (2)$$

In the formula, Δh is the length of cube pixels, and the average infiltration depth (*ID*) of each group of experiments is taken, and calculated as Formula (3). The infiltration uniformity (S2) of soil moisture is further analyzed and calculated as Formula (4).

$$\overline{ID} = \overline{H_a(x, y)} = \frac{\sum_{i=1}^{n} a(x_i, y_i, z_i)\Delta h}{xy} \quad (3)$$

$$S^2 = \frac{1}{n}\left[\sum_{i=1}^{n}\left[H_a(x,y) - \overline{H_a(x,y)}\right]^2\right] \quad (4)$$

The preferential flow ratio (*PF-fr*) and the contribution of preferential flow infiltration to total infiltration are the main parameters for analyzing the preferential flow characteristics of the soil.

The preferential flow ratio is calculated as follows:

$$PF - fr = 100 \cdot \left(1 - \frac{Unifr \cdot X}{TSA}\right) \quad (5)$$

In the formula, *UniFr* is the uniform infiltration depth (infiltration depth when the dyed area reaches 80%), *X* is the profile width (100 cm in this research), and *TSA* is the total area of the dyed region.

The preferential flow infiltration volume (*PIV*) and its contribution to the total infiltration. PIV is preferential flow infiltration volume and is calculated as follows:

$$PIV = \sum_{i=0}^{i=ID} Vi - \sum_{j=0}^{j=Unifr} Vj \quad (6)$$

In the formula, *Vi* and *Vj* are the infiltration volumes of soil moisture at depths *I* and j respectively, and are calculated as follows:

$$V = \sum_{U=1}^{U=8}(\theta tu - \theta iu)\mathrm{Vs/U} \quad (7)$$

In the formula, θtu is the water content of the soil after rainfall, θiu is the water content of the initial soil, U is the sequence number of each layer of the soil sample, and VS is the soil volume. The *contribution* (%) of preferential flow infiltration can be defined as the ratio of preferential flow infiltration volume (*PIV*) to total infiltration volume (*TIV*) and is calculated as follows:

$$Contribution = 100 \cdot \frac{PIV}{TIV} \quad (8)$$

3. Results

3.1. Soil Water Infiltration Depth

In order to reflect the spatial distribution characteristics of the infiltration depth, infiltration depth information was programmed using the mesh function of the MATLAB software to obtain an infiltration distribution map of each experiment area. As shown in Figures 5–7, the color change in the stain strip represents the depth of soil water infiltration. In Figure 7, the influence of the fracture network on soil water infiltration depth is clearly reflected by drawing an infiltration depth map. Combined with the infiltration distribution map, the influence of rainfall intensity, rainfall duration, and cracks on solute migration was analyzed using the average infiltration depth, and the uniformity of solute migration was analyzed with average infiltration depth variance.

In experiment S1, when the infiltration volume was 10 L, the average infiltration depths of S1-1, S1-2, and S1-3 were 2.55 cm, 2.65 cm, and 2.44 cm, respectively, and the variances were 6.5, 7.7, and 4.2, respectively. When the infiltration volume was 20 L, the average infiltration depths of S1-4, S1-5, and S1-6 were 5.33 cm, 5.65 cm, and 3.94 cm, respectively, and the variances were 12.2, 12.5, and 7.5, respectively. When the infiltration volume was 30 L, the average infiltration depth of S1-7 was 7.36 cm, and the variance was 20.0. The infiltration depth of 30 L increased by 4.71 cm compared with that of the 10 L infiltration. As can be seen from Figure 5, when the infiltration water increased, the average infiltration depth also increased, and the infiltration uniformity became worse. With the same infiltration water, the nonfractured experiment using a landfill treatment was smaller in terms of the average infiltration depth compared with the fractured experiment without a landfill treatment, and the infiltration was uniform.

In experiment S2, the average infiltration depths of S2-1, S2-2, S2-3, and S2-4 were 6.13 cm, 12.27 cm, 12.97 cm, and 26.14 cm, respectively, and the variances were 4.0, 5.5, 15.0, and 49.6 respectively. As can be seen from Figure 6, when the rainfall intensity was 20 mm/h, and the rainfall duration was 20 min, the average infiltration depth was shallow, the water infiltration was uniform, and the preferential flow began to develop and form. However, the matrix flow area was larger, and the preferential flow only developed locally. When the rainfall intensity was 50 mm/h, and the rainfall duration was 50 min, the partial infiltration depth exceeded the depth of the fractures and the water infiltration was very uneven. In this case, there were more preferential flow channels and better preferential flow developments. The increase in rainfall intensity and rainfall duration increased the average infiltration depth and the infiltration uniformity.

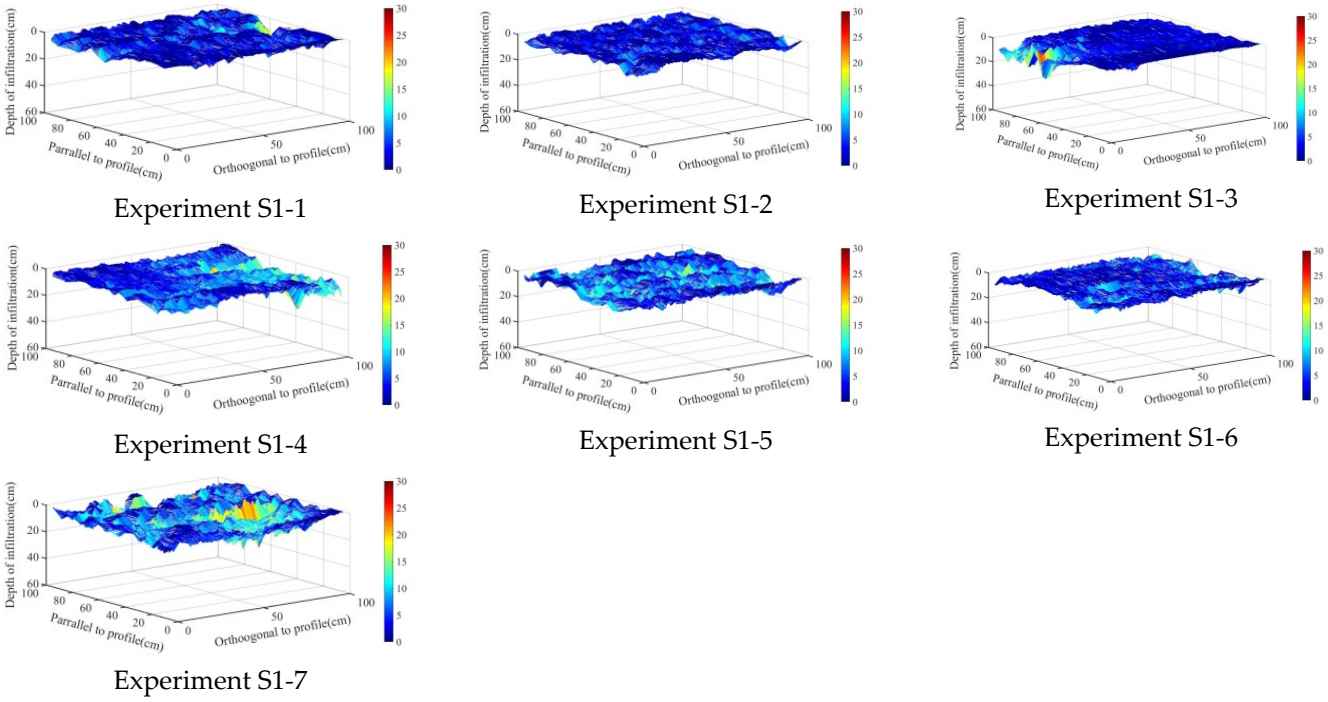

Figure 5. Spatial distribution of infiltration depth under experiment S1.

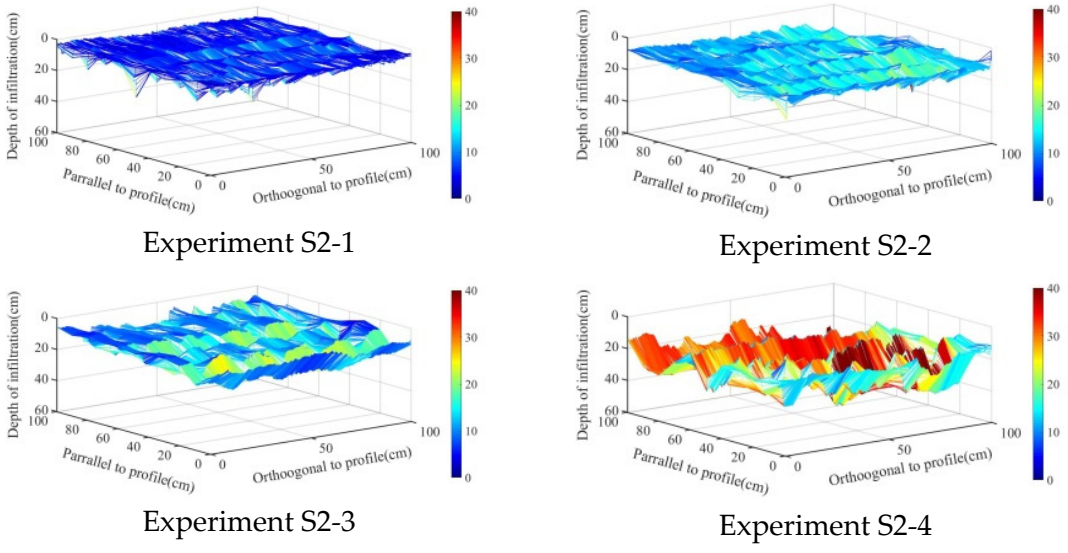

Figure 6. Spatial distribution of infiltration depth under experiment S2.

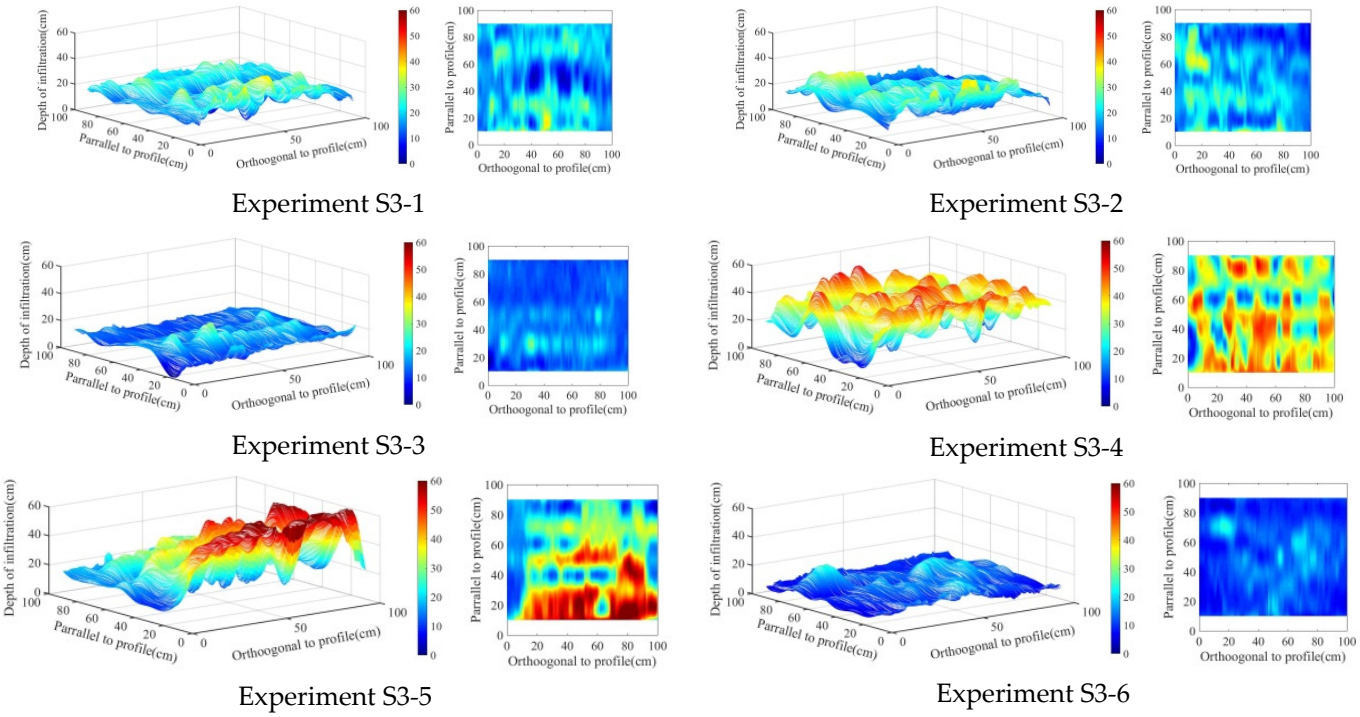

Figure 7. Spatial distribution of infiltration depth under experiment S3.

In experiment S3, the non-crack comparative experiment, the inclined slope with the horizontal, 10° angle was added in order to restore the real situation in the field. The average infiltration depths of S3-1, S3-2, and S3-3 were, respectively, 20.32 cm, 18.45 cm, and 13.69 cm, with a rainfall intensity of 30 mm/h and a rainfall duration of 60 min. The variances were 20.5, 25.5, and 5.6, respectively. The average infiltration depths of the S3-4, S3-5, and S3-6 treatments were, respectively, 33.46 cm, 32.49 cm, and 11.64 cm, with a rainfall intensity of 50 mm/h and a rainfall duration of 30 min. The variances were 74.9, 108.4, and 8.6, respectively. Compared with the non-crack experiment group, the average infiltration depth of the crack experiment group under a precipitation intensity of 30 mm/h was 5.70 cm, and at 50 mm/h, it was 21.34 cm. As can be seen from the cloud image in Figure 7, the mesh lines of the fractured area became thicker, the color changed from blue to red along the fractured network after the 50 mm/h treatment, and the mesh integrity was good. The color of the matrix area was mostly blue, and the color changed irregularly. Compared with the control treatment without cracks, the increase in rainfall intensity and the extension of rainfall duration both contributed to the formation of preferential flow, but the increase in rainfall intensity had a more dramatic effect on the uniformity of infiltration than the extension of rainfall duration. Therefore, rainfall intensity may be the primary factor for the development of preferential flow. This phenomenon may be attributed to the unbalanced characteristics of the preferential flow; that is, the water flux in the preferential flow path is higher than in the soil matrix, and the rapid flow characteristics of the preferential flow cause the soil water infiltration to bypass the soil matrix and infiltrate rapidly along the cracks. The higher the rainfall intensity, the faster the soil surface water content reaches saturation. The cracks played an important role in soil water infiltration, and they can be used as the priority flow path to increase soil water infiltration.

3.2. Dye Coverage

Establishing the dyeing area ratio is an intuitive and quantitative way of describing the trajectory of preferential flow in a vertical profile. By drawing different layers in the vertical direction, the three-dimensional spatial distribution of the preferential flow can be obtained [20]. In experiment S2, the average dyeing areas of the S2-1, S2-2, S2-3, and S2-4 treatments were 10.2%, 20.5%, 21.6%, and 41.7%, respectively. As can be seen from Figure 8,

the average dyeing area ratio with different treatments decreased with the increase in the infiltration depth, indicating the infiltration process was not balanced and that there was a preferential flow phenomenon. The average dyeing area increased with the increase in rainfall intensity and rainfall duration. When the rainfall intensity was 20 mm/h, the average dyeing area decreased slowly with the increase in infiltration depth, and then, it decreased to zero rapidly. At this point, only a small part of the preferential flow was developed, and the soil water infiltration was mainly dominated by matrix flow. When the rainfall intensity was 50 mm/h, and the rainfall duration was 50 min, the curve of the average dyeing area changed slowly with the infiltration depth. At this point, the preferential flow was well developed, there was more preferential flow path, and the preferential flow was larger.

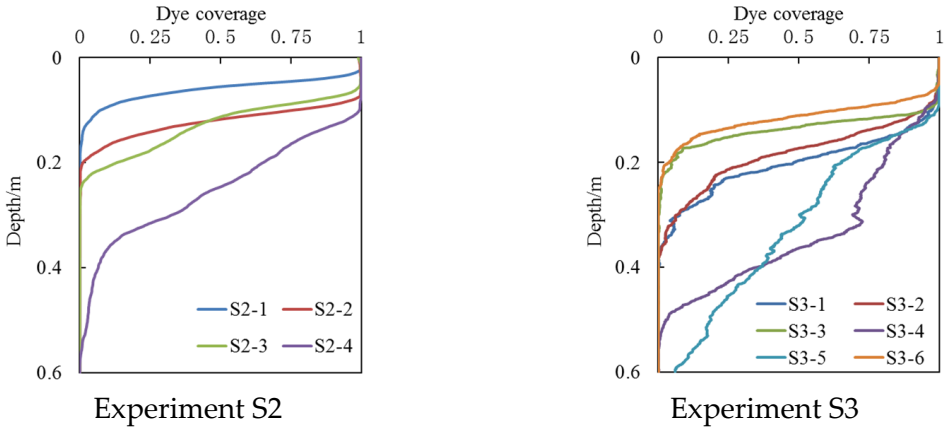

Figure 8. Dye coverage distributions.

In experiment S3, the average dyeing areas of the S3-1, S3-2, and S3-3 treatments were 33.9%, 30.7%, and 22.8%, respectively. The average dyeing areas of the S3-4, S3-5, and S3-6 treatments were 55.8%, 54.2%, and 19.0%, respectively. Compared with the non-crack experiment group, the average dyeing areas of the crack experiment group under a precipitation intensity of 30 mm/h was 9.5%, and at 50 mm/h, it was 36%. With the same rainfall intensity, the presence of cracks increased the preferential flow path and, thus, increased the average dyeing area, confirming that cracks are the major contributors to the preferential flow. When the rainfall intensity was 50 mm/h, and the rainfall duration was 30 min, the curve of the average dyeing area after dyeing fluctuated with the increased infiltration depth in the S3-4 and S3-5 treatments. At this time, the lateral flow of soil moisture occurred, which was not significant with a rainfall intensity of 30 mm/h during the S3-6 treatment.

3.3. Soil Saturation

The soil samples taken by the experiment were measured via the drying method, and soil water infiltration was analyzed by saturation. The initial saturation and the saturation after rainfall showed a V-type distribution; the initial saturation increased with depth, and it stabilized at a certain depth. The soil saturation then decreased with the depth after rainfall, and it stabilized at a certain depth; that is, the initial saturation of the soil was reached. The depth of the V-type is closely related to the soil water infiltration model. The V-type is mainly dominated by the matrix flow at a shallow depth, and when the V-type is deep, the preferential flow will be better developed.

In experiment S2, as seen in Figure 9, when rainfall was 20 mm/L, the saturation of the interval also increased from 0 to 0.3 Z_{max} (Z_{max} is the maximum infiltration depth) with the increase in duration. At 0.3 Z_{max}, the saturation curve after rainfall gradually intersected with the initial saturation curve. When the rainfall duration increased, the saturation after rainfall increased, but the infiltration depth did not increase obviously, and the soil water infiltration was mainly based on the matrix flow. When the rainfall intensity was 50 mm/h,

and the rainfall duration was 50 min, the saturation curve after rainfall intersected the initial saturation curve at 0.6 Z_{max}. At this time, there was a deep soil water infiltration depth with more infiltration, and preferential flow was better developed.

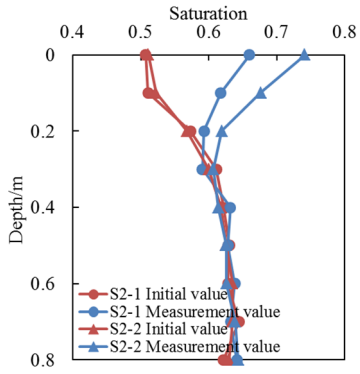

Experiment S2 rain with an intensity of 20 mm·h^{-1}

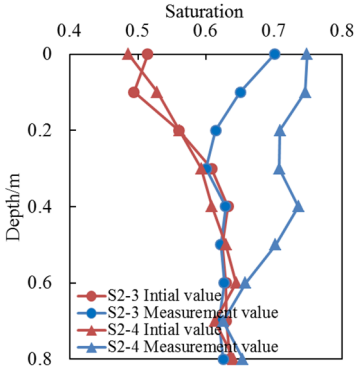

Experiment S2 rain with an intensity of 50 mm·h^{-1}

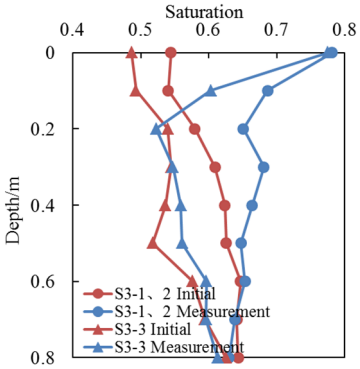

Experiment S3 rain with an intensity of 30 mm·h^{-1}

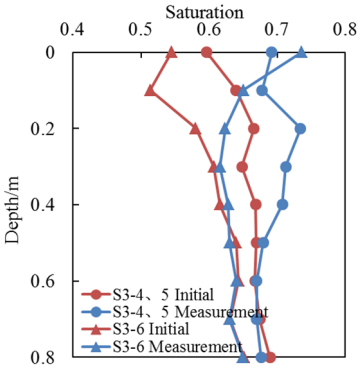

Experiment S3 rain with an intensity of 50 mm·h^{-1}

Figure 9. Comparison of measured saturation.

In experiment S3, we averaged the two groups of cracked replicates at 30 mm/h and 50 mm/h and analyzed the behavior of soil water infiltrations in the presence of fractures by comparing them with the nonfractured experiment. As can be seen from Figure 9, although the initial soil water content was different, the infiltration depth of the fracture treatment was obviously deeper than that of the nonfractured treatment. The saturation curve of the fracture treatment after rainfall at 30 mm/h intersected with the initial saturation curve at 0.6 Z_{max}, while the non-fractured treatment intersected at 0.2 Z_{max}. At 50 mm/h, the saturation curve of the fracture treatment after rainfall intersected with the initial saturation curve at 0.6 Z_{max}, while the non-fractured treatment intersected at 0.1 Z_{max}.

3.4. The Influence of the Fracture Network on the Runoff

When the rainfall intensity was 30 mm/h, the slope flow formation times of the S3-1, S3-2, and S3-3 treatments were, respectively, 2294, 3147, and 1279 s after the start of the simulated rainfall. After the rainfall ended, the total water amounts collected during the slope flow were 6300, 815, and 7960 mL, respectively. The slope flow generation times of the S3-4, S3-5, and S3-6 treatments were 741, 819, and 350 s, respectively, and the total slope flow water amounts were 11,790, 6500, and 19,650 mL. Compared with the non-crack experiment group, the slope flow formation time of the crack experiment group under a precipitation intensity of 30 mm/h was 430 s, and at 50 mm/h, it was 1441.5 s.

The rainfall infiltration coefficient refers to the ratio of infiltration and precipitation, and the runoff coefficient refers to the ratio of runoff and rainfall. It can be seen from Table 3 that the runoff coefficients of the S3-1, S3-2, and S3-3 treatments at 30 mm/h were 0.2100, 0.0272, and 0.2653, respectively, and the rainfall infiltration coefficients were 0.7900, 0.9728, and 0.7347. The runoff coefficients of the S3-4, S3-5, and S3-6 treatment at 50 mm/h were

0.4716, 0.2600, and 0.7860, respectively, and the rainfall infiltration coefficients were 0.5284, 0.7400, and 0.2140, respectively. Compared with the non-crack experiment group, the runoff coefficients of the crack experiment group under a precipitation intensity of 30 mm/h was 0.15, and at 50 mm/h, it was 0.42. These results show that, when the rainfall intensity is the same, the fractures reduce the runoff coefficient, increase the rainfall infiltration coefficient, reduce the slope flow, and increase the infiltration capacity of the soil water. When the rainfall intensity increases, the runoff coefficient increases, the rainfall infiltration coefficient decreases, the slope flow increases, and the soil water infiltration decreases.

Table 3. Runoff and infiltration coefficients.

Experiment Label	Runoff Amount/mL	Infiltration Amount/mL	Runoff Coefficient	Infiltration Coefficient
S3-1	6300	23,700	0.2100	0.7900
S3-2	815	29,185	0.0272	0.9728
S3-3	7960	22,040	0.2653	0.7347
S3-4	11,790	13,210	0.4716	0.5284
S3-5	6500	18,500	0.2600	0.7400
S3-6	19,650	5350	0.7860	0.2140

4. Discussion

4.1. Expression of Phenomenon Result

The study of solute migration shows that revealing its essential laws and constructing mathematical models are inseparable from the correct analysis of its phenomena. In experiment S1, the experimental results were consistent with previous studies: The increase in infiltration promoted the development of preferential flow [43,44]. Preferential flow refers to the phenomenon where water flows rapidly and downwardly around the soil matrix through cracks and macropores, which is a common form of water flow and solute migration in soil [45,46]. When the rainfall intensity increases, the solute migration rate will increase correspondingly; that is, the larger the infiltration capacity, the deeper the solute migration depth of soil water. Under natural conditions, the evolution of cracks is a complicated and lengthy process. In experiment S1, cracks were formed by natural shrinkage after watering. Soil tends to expand after watering; some cracks close, and the water infiltration rate decreases gradually [47]. The fast and heterogeneous soil expands, and the preferential flow caused by the fracture only lasts for hours [48]. The variance in the mean infiltration depth of experiment S1 was smaller, and infiltration was more uniform. Although preferential flow paths exist with only a small amount of water, most soil water is permeated through the soil matrix, and the phenomenon of preferential flow is not obvious.

In experiment S2, when the raininess was 20 mm/h, the infiltration depth increased with the increase in rainfall time, and the preferential flow began to develop and form; however, the matrix flow area was larger, so the preferential flow only developed locally. When the raininess was 50 mm/h and rainfall time was 20 min, the main motion path of the water flow was the crack channels; it bypassed the soil matrix and rapidly moved until it reached the deep soil, and there was an obvious preferential flow phenomenon. When the time increased to 50 min, the infiltration depth exceeded the depth of the cracks. At this point, the cracks did not play a major role in soil moisture movement, and the area had complete color development. The test results were consistent with previous research results [49,50]; namely, the lower the intensity of rainfall or irrigation is, the more easily the soil water passes through this area in the form of matrix flow, and, conversely, the more preferential the flow channels are, the larger the preferential flow is. This shows that increased rainfall or irrigation intensity can promote the activation of preferential channels, which is beneficial to the formation of preferential flow.

In experiment S3, soil solute migration under rainfall conditions included two processes: first of all, the soil solute infiltrated and migrated toward the deep soil, along with water infiltration in the rainfall process. Secondly, when the raininess was greater than

the soil water infiltration capacity, it produced direct surface runoff, and the surface soil solute migrated along with the direct surface runoff and under the scouring action of the runoff. Although the average infiltration depth and average dyed area could not be used to evaluate the contribution of the preferential flow to the soil water infiltration [51], they are useful methods to intuitively and quantitatively describe the movement locus of preferential flow in a vertical section. By drawing different sections in the vertical direction, the 3D spatial distribution characteristics of the preferential flow were obtained. Then, one can generate the runoff time and the average runoff coefficient, as well as intuitively and quantitatively describe the effect of slope surface and cracks on the preferential flow.

4.2. Analysis of Phenomenon Result

In Table 4, the characteristics of soil preferential flow of S2 and S3 experiments are counted. In the four groups of experiments with S2 non-sloped treatment, the contribution of preferential flow infiltration to total infiltration was more than 40%, and there was a strong phenomenon of preferential flow in soil water infiltration, and the contribution of preferential flow infiltration to total infiltration was more significant than the increase of rainfall intensity compared with the increase of rainfall duration. The increase in rainfall or irrigation intensity could make the cracks become infiltration channels and increase the water flux in the preferential flow path. The rainfall intensity and rainfall duration with S2-1 treatment were small, and the characteristic values of preferential flows were low. In the S2-2 treatment, the characteristic values of preferential flows increased significantly with the increase in rainfall duration, and the average infiltration depth and maximum infiltration depth changed significantly. S2-3 treatment increased the rainfall intensity, but the total rainfall was the same as that of S2-2. It can be found that the infiltration becomes uneven with the increase of rainfall intensity, and the values of preferential flow ratio and contribution of preferential flow infiltration to the total infiltration both increased significantly. In the S2-4 treatment, the rainfall intensity and rainfall duration were the maxima in the experiment, and its characteristic values of preferential flows were also the peak. Comparing S2-2 and S2-3 experiments, it can be found that the increase of both rainfall intensity and rainfall duration contributes to the formation of preferential flow, but the promotion effect of rainfall intensity is more significant.

Table 4. Characteristics (i.e., *ID, Unifr, Contribution* etc.) of soil preferential flow.

Experiment Label	$\overline{ID}$	ID	S^2	Unifr	DC	PF-fr	Contribution
S2-1	6.13	26.90	4.00	4.90	10.20	19.90	40.00
S2-2	12.27	41.80	5.50	9.70	20.50	21.10	41.60
S2-3	12.97	34.40	15.00	8.40	21.60	35.20	52.00
S2-4	26.14	58.60	49.60	15.00	41.70	40.00	58.40
S3-1	20.30	39.80	20.50	15.40	33.90	24.30	48.00
S3-2	18.50	38.30	25.50	13.30	30.70	27.80	47.10
S3-3	13.70	30.20	5.60	11.30	22.80	17.40	16.30
S3-4	33.50	55.50	74.90	20.60	55.80	38.50	50.30
S3-5	32.50	60.00	108.40	15.80	54.20	51.40	70.30
S3-6	11.60	25.10	8.60	8.80	19.00	22.80	26.70

Among the six groups of experiments with S3 sloped treatment, the contribution of preferential flow infiltration to total infiltration was 16.30% and 26.70% for the S3-3 and S3-6 non-cracked groups, which was due to the absence of soil cracks, but there were still other preferential flow paths such as macropores, which were also significantly promoted by the increase of rainfall intensity. The experimental results show that soil cracks on slopes play an important role in rainfall redistribution, and the existence of cracks increases the infiltration of soil water while reducing the surface runoff volume and delaying the time of surface runoff formation. At the same time, the uniform infiltration depth, the average dyed area, the preferential flow ratio, and the contribution of preferential flow

infiltration to total infiltration are increased. Compared with the treatment without cracks, the uniform infiltration depth increased by 9.4 cm, the average dyed area increased by 36.0%, the preferential flow ratio increased by 8.7%, and the contribution of preferential flow infiltration to total infiltration increased by 31.3% in the treatment group with cracks at a rainfall intensity of 50 mm/h. The uniform infiltration depth increased by 3.1 cm, the average dyed area increased by 9.5%, the preferential flow ratio increased by 22.2%, and the contribution of preferential flow infiltration to total infiltration increased by 33.6% in the treatment group with cracks at a rainfall intensity of 30 mm/h. Both rainfall duration and rainfall intensity can promote the activation of cracked channels as preferential flow channels, which is conducive to the formation of preferential flow. When the rainfall intensity increases, the formation of preferential flow is faster and does not inhibit the formation of matrix flow. When the rainfall duration increases, the matrix flow area increases and also promotes the formation of preferential flow.

4.3. Research Implications

Due to the unbalanced, fast-moving, and lateral infiltration characteristics of the preferential flow, Darcy's law cannot be used to calculate water flux and solute movement time. Niu et al. [52] compared the water flux along the preferred flow path with the soil matrix using the soil column test and concluded that the water flux fluctuates with time; however, the water flux in the preferred flow path is higher than in the soil matrix. Fissure flow, as a kind of preferential flow, is common in croplands with clay soil. Fissures can be used as priority channels to accelerate water infiltration in the process of irrigation or rainfall, which not only reduces the utilization efficiency of water and fertilizer, but also leads to the infiltration of phosphorus [53–55], cadmium [56], and other pollutants into the groundwater layer. This may also cause secondary salinization disasters.

At the same time, slope soil fissures play a crucial role in redistributing precipitation to surface runoff and soil water infiltration. Slope soil fissures help slow down the formation of surface runoff, thus affecting soil water infiltration and lateral flow [57]. When rainwater enters the fractured soil from the slope surface, it will flow in the fractured network and penetrate the soil matrix. In the preferred flow path, the internal soil will erode, and the soil shear strength will reduce, thus affecting slope stability [58]. At the same time, the dynamic parameters of surface runoff are also affected by factors such as soil shrinkage cracks, unit discharge, and Reynolds number reduction. In addition, by changing the division of rainfall between seepage and runoff, soil fissures have a significant impact on surface flow movement and flood dynamics, which is an important issue to be considered in the simulation and prediction of flood events. Therefore, studying the influence of soil cracks on surface runoff and seepage has practical significance in understanding the physical basis of non-uniform soil flow and simulating non-uniform flow.

5. Conclusions

In this study, 17 dye tracer experiments were conducted in the field in three groups according to differences in fractures, rainfall intensity, rainfall duration, and slope. The effects of fracture, rainfall intensity, rainfall duration, and slope surface on solute migration and farmland runoff were analyzed through the parameters of infiltration depth, dyeing area, saturation, runoff coefficient, and rainfall infiltration coefficient. Experiment S1 showed that increasing the infiltration rate promoted the migration rate of the solute and the instability of natural shrinkage cracks, and the fractures gradually closed for another watering to reduce the solute migration rate. Experiment S2 showed that increasing the rainfall or irrigation intensity promoted the activation of the fracture channel as the preferential flow channel, which was advantageous to the preferential flow formation. The results of experiment S3 showed that the cracks were dominant in the development of preferential flow, and the existence of cracks slowed the formation of runoff, reduced the velocity of slope flow, reduced the flow of slope, and increased the infiltration of soil water. The results improved the understanding of water movement and solute migration behavior

in the field and have important application values in guiding agricultural irrigation and improving the efficiency of agricultural water use.

This research was an in situ field experiment with an artificial soil crack network as a research object. In the cropland growing fields, models of land desiccation crack networks are very complex. Their characters change with the presence of water and their influences on solute movement also change. The scope of the crack network, spatial structure, and positions of the start point and termination point need to be determined through massive experiments. Although the dye tracer test method can directly describe the characteristics and inherent behavior of solute transport phenomena, it cannot analyze the dynamic process of preferential flow movement based on rainfall duration. Therefore, the focus of future research should be on how to monitor dynamic changes in the soil moisture content of crack and non-crack areas and the establishment of a numerical model.

Author Contributions: Conceptualization, J.Y.; methodology, J.Y. and S.W.; validation, J.Y., S.W. and D.X.; data curation, J.Y., S.W. and D.X.; writing—original draft preparation, J.Y.; writing—review and editing, S.W. and D.X. All authors have read and agreed to the published version of the manuscript.

Funding: This research was financially supported by grants from the National Science Foundation of China (No. 51569023 and 51369025) and the Postgraduate Innovation Funding Project of Hebei Province (No. CXZZBS2021018).

Institutional Review Board Statement: Not applicable.

Informed Consent Statement: Not applicable.

Data Availability Statement: The datasets used and/or analyzed during the current study are available from the corresponding author upon reasonable request.

Acknowledgments: The authors would like to express their gratitude to the Hebei University of Engineering.

Conflicts of Interest: The authors declare no conflict of interest.

References

1. Lu, Y.; Liu, S.; Weng, L.; Wang, L.; Li, Z.; Xu, L. Fractal analysis of cracking in a clayey soil under freeze–thaw cycles. *Eng. Geol.* **2016**, *208*, 93–99. [CrossRef]
2. Zhang, Z.B.; Peng, X.H. A review of researches on soil cracks and their impacts on preferential flow. *Acta Pedol. Sin.* **2015**, *52*, 477–488.
3. Peng, X.; Horn, R.; Smucker, A. Pore Shrinkage Dependency of Inorganic and Organic Soils on Wetting and Drying Cycles. *Soil Sci. Soc. Am. J.* **2007**, *71*, 1095–1104. [CrossRef]
4. Tang, C.; Shi, B.; Liu, C.; Zhao, L.; Wang, B. Influencing factors of geometrical structure of surface shrinkage cracks in clayey soils. *Eng. Geol.* **2008**, *101*, 204–217. [CrossRef]
5. Zhang, Z.; Peng, X.; Wang, L.; Zhao, Q.; Lin, H. Temporal changes in shrinkage behavior of two paddy soils under alternative flooding and drying cycles and its consequence on percolation. *Geoderma* **2013**, *192*, 12–20. [CrossRef]
6. Niu, J.Z.; Yu, X.X.; Zhang, Z.Q. The present and future research on preferential flow. *Acta Ecol. Sin.* **2006**, *26*, 231–243.
7. Vogel, H.J.; Hoffmann, H.; Leopold, A. Studies of crack dynamics in clay soil: II. A physically based model for crack formation. *Geoderma* **2005**, *125*, 213–223. [CrossRef]
8. Krisnanto, S.; Rahardjo, H.; Fredlund, D.G.; Leong, E.C. Mapping of cracked soils and lateral water flow characteristics through a network of cracks. *Eng. Geol.* **2014**, *172*, 12–25. [CrossRef]
9. Klaus, J.; Zehe, E.; Elsner, M.; Palm, J.; Schneider, D.; Schröder, B.; Steinbeiss, S.; Van Schaik, L.; West, S. Controls of event-based pesticide leaching in natural soils: A systematic study based on replicated field scale irrigation experiments. *J. Hydrol.* **2014**, *512*, 528–539. [CrossRef]
10. Radolinski, J.; Le, H.; Hilaire, S.S.; Xia, K.; Scott, D.; Stewart, R.D. A spectrum of preferential flow alters solute mobility in soils. *Sci. Rep.* **2022**, *12*, 4261. [CrossRef]
11. Reichenberger, S.; Amelung, W.; Laabs, V.; Pinto, A.; Totsche, K.U.; Zech, W. Pesticide displacement along preferential flow pathways in a Brazilian Oxisol. *Geoderma* **2002**, *110*, 63–86. [CrossRef]
12. Jarvis, N.J. A review of non-equilibrium water flow and solute transport in soil macropores: Principles, controlling factors and consequences for water quality. *Eur. J. Soil Sci.* **2007**, *58*, 523–546. [CrossRef]
13. Zhan, L.T.; Jia, G.W.; Chen, Y.M.; Fredlund, D.G. Analytical solution for rainfall infiltration into infinite long slopes considering properties of unsaturated soil. *Chin. J. Geotech. Eng.* **2010**, *32*, 1214–1220.

14. Zhang, J.; Ming, L.; Yi, Z.Z.; Chong, L.; Chikhotkin, V.; Fei, Z.Y. Effects of preferential flow induced by desiccation cracks on the slope stability. *Eng. Geol.* **2021**, *288*, 106164. [CrossRef]
15. Hu, H.C.; Wen, J.; Peng, Z.Y.; Tian, F.Q.; Tie, Q.; Lu, Y.; Khan, M.Y.A. High-frequency monitoring of the occurrence of preferential flow on hillslopes and its relationship with rainfall features, soil moisture and landscape. *Hydrol. Sci. J.* **2019**, *64*, 1385–1396. [CrossRef]
16. Zhang, X.N.; Feng, J.; Zhang, C. Influence of soil macropore on hydrodynamic parameters of overland flow with different rainfall intensities. *J. Hohai Univ. Nat. Sci.* **2012**, *40*, 264–269.
17. Zhang, Z.B.; Zhou, H.; Zhao, Q.G.; Lin, H.; Peng, X. Characteristics of cracks in two paddy soils and their impacts on preferential flow. *Geoderma* **2014**, *228–229*, 114–121. [CrossRef]
18. Laine-Kaulio, H.; Backnäs, S.; Koivusalo, H.; Laurén, A. Dye tracer visualization of flow patterns and pathways in glacial sandy till at a boreal forest hillslope. *Geoderma* **2015**, *259–260*, 23–34. [CrossRef]
19. Sheng, F.; Liu, H.; Wang, K.; Zhang, R.; Tang, Z. Investigation into preferential flow in natural unsaturated soils with field multiple-tracer infiltration experiments and the active region model. *J. Hydrol.* **2014**, *508*, 137–146. [CrossRef]
20. Flury, M.; Flühler, H. Modeling Solute Leaching in Soils by Diffusion-Limited Aggregation: Basic Concepts and Application to Conservative Solutes. *Water Resour. Res.* **1995**, *31*, 2443–2452. [CrossRef]
21. Flury, M.; Wai, N.N. Dyes as tracers for vadose zone hydrology. *Rev. Geophys.* **2003**, *41*, 1002. [CrossRef]
22. Hatano, R.; Kawamura, N.; Ikeda, J.; Sakuma, T. Evaluation of the effect of morphological features of flow paths on solute transport by using fractal dimensions of methylene blue staining pattern. *Geoderma* **1992**, *53*, 31–44. [CrossRef]
23. Nobles, M.M.; Wilding, L.P.; Lin, H.S. Flow pathways of bromide and Brilliant Blue FCF tracers in caliche soils. *J. Hydrol.* **2010**, *393*, 114–122. [CrossRef]
24. Zhu, L.; Chen, J.H.; Liu, D.D. Preferential flow model coupling soil matrix with fracture network and its validation. *Trans. Chin. Soc. Agric. Eng.* **2016**, *32*, 15–21.
25. Sheng, F.; Wang, K.; Zhang, R.; Liu, H. Characterizing soil preferential flow using iodine–starch staining experiments and the active region model. *J. Hydrol.* **2009**, *367*, 115–124. [CrossRef]
26. Flury, M.; Flühler, H. Brilliant Blue FCF as a Dye Tracer for Solute Transport Studies—A Toxicological Overview. *J. Environ. Qual.* **1994**, *23*, 1108–1112. [CrossRef]
27. Wang, K.; Zhang, R. Heterogeneous soil water flow and macropores described with combined tracers of dye and iodine. *J. Hydrol.* **2011**, *397*, 105–117. [CrossRef]
28. Kutilek, M.; Germann, P.F. Converging hydrostatic and hydromechanic concepts of preferential flow definitions. *J. Contam. Hydrol.* **2008**, *104*, 61–66. [CrossRef]
29. Lin, H.; Gilkes, R.J.; Prakongkep, N. Linking principles of soil formation and flow regimes. *J. Hydrol.* **2010**, *393*, 3–19. [CrossRef]
30. Zhang, J.Y.; Liu, T.X.; Duan, L.M.; Chen, Z.X.; Wang, Y.X.; Li, Y.K.; Zhao, X.Y.; Wang, G.Q.; Singh, V.P. Processes of preferential flow in a eurasian steppe under different scenarios. *J. Hydrol.* **2022**, *612*, 128166. [CrossRef]
31. Li, M.F.; Yao, J.J.; Yan, R.; Cheng, J.H. Effects of Infiltration Amounts on Preferential Flow Characteristics and Solute Transport in the Protection Forest Soil of Southwestern China. *Water* **2021**, *13*, 1301. [CrossRef]
32. Li, M.F.; Yao, J.J.; Yan, R.; Cheng, J.H. Study on the Preferential Flow Characteristics under Different Precipitation Amounts in Simian Mountain Grassland of China. *Water* **2020**, *12*, 3489. [CrossRef]
33. Li, Y.M.; Werner, A.D.; Wen, Z.; Zhu, Q. Solute transport in permeable porous media containing a preferential flow feature: Investigation of non-Darcian flow effects. *J. Hydrol.* **2022**, *604*, 127210. [CrossRef]
34. Lu, D.B.; Wang, H.; Geng, N.; Xia, Y.F.; Xu, C.D.; Hua, E. Imaging and characterization of the preferential flow process in agricultural land by using electrical resistivity tomography and dual-porosity model. *Ecol. Indic.* **2022**, *134*, 108498. [CrossRef]
35. Vilim, F.; Jasmina, D.; Jiří, Š.; Lana, F.; Gabrijel, O.; Davor, R.; Igor, B.; Ivan, M.; Josip, Ć.; Radka, K. Estimation of vineyard soil structure and preferential flow using dye tracer, X-ray tomography, and numerical simulations. *Geoderma* **2020**, *380*, 114699.
36. Holbak, M.; Abrahamsen, P.; Hansen, S.; Diamantopoulos, E. A Physically Based Model for Preferential Water Flow and Solute Transport in Drained Agricultural Fields. *Water Resour. Res.* **2021**, *57*, e2020WR027954. [CrossRef]
37. Švob Mirna Domínguez, V.D.; Krklec, K. Characterization of soil drainage dynamics on karst terrains by developing a site-specific reservoir cascade scheme hydrological model with preferential flows. *J. Hydrol.* **2022**, *612*, 128147. [CrossRef]
38. Zhang, J. An efficient median filter based method for removing random-valued impulse noise. *Digital Signal Process.* **2010**, *20*, 1010–1018. [CrossRef]
39. Hua, S.; Chen, Y.; Liang, L.; Ren, T. Studying soil pore structure by using image filtering technology based on partial differential equation model. *Trans. Chin. Soc. Agric. Eng.* **2014**, *30*, 78–85.
40. Kramers, G.; Richards, K.G.; Holden, N.M. Assessing the potential for the occurrence and character of preferential flow in three Irish grassland soils using image analysis. *Geoderma* **2009**, *153*, 362–371. [CrossRef]
41. Wang, K.; Zhang, R.; Yasuda, H. Characterizing heterogeneity of soil water flow by dye infiltration experiments. *J. Hydrol.* **2006**, *328*, 559–571. [CrossRef]
42. Pan, W.S.; Xu, Y.F.; Lu, Y.D.; Gao, L.; Xin, Y. Quantitative determination of preferential flow characteristics of loess based on nonuniformity and fractional dimension. *Trans. Chin. Soc. Agric. Eng.* **2017**, *33*, 140–147.
43. Sheng, F.; Fang, Y. Study on Preferential Soil Water Flow Using Iodine-starch Staining Method. *Soils* **2012**, *44*, 144–148.

44. Wu, Q.; Liu, C.; Lin, W.; Zhang, M.; Wang, G.; Zhang, F. Quantifying the Preferential Flow by Dye Tracer in the North China Plain. *J. Earth Sci.* **2015**, *26*, 435–444. [CrossRef]
45. Liu, H.H.; Zhang, R.; Bodvarsson, G.S. An active region model for capturing fractal flow patterns in unsaturated soils: Model development. *J. Contam. Hydrol.* **2005**, *80*, 18–30. [CrossRef]
46. Beven, K.; Germann, P. Macropores and water flow in soils. *Water Resour. Res.* **1982**, *18*, 1311–1325. [CrossRef]
47. Liu, C.W.; Cheng, S.W.; Yu, W.S.; Chen, S.K. Water infiltration rate in cracked paddy soil. *Geoderma* **2003**, *117*, 169–181. [CrossRef]
48. Favre, F.; Boivin, P.; Wopereis, M.C.S. Water movement and soil swelling in a dry, cracked Vertisol. *Geoderma* **1997**, *78*, 113–123. [CrossRef]
49. Trojan, M.D.; Linden, D.R. Microrelief and Rainfall Effects on Water and Solute Movement in Earthworm Burrows. *Soil Sci. Soc. Am. J.* **1992**, *56*, 727–733. [CrossRef]
50. Gjettermann, B.; Nielsen, K.L.; Petersen, C.T. Preferential flow in sandy loam soils as affected by irrigation intensity. *Soil Technol.* **1997**, *11*, 139–152. [CrossRef]
51. Wu, J.Q.; Zhang, J.F.; Gao, R. Physical simulation experiments of effects of macropores on soil water infiltration characteristics. *Trans. Chin. Soc. Agric. Eng.* **2009**, *25*, 13–18.
52. Niu, J.Z.; Xia, X.Y.U.; Zhang, Z.Q. Analysis of solute preferential transport in a dark coniferous forest ecosystem of Gongga Mountain, Sichuan Province, southwestern China. *For. Ecosyst.* **2010**, *12*, 14–20. [CrossRef]
53. Vera, M.; Stefan, J.; Karl, H.F.; Dorit, J. Soil Phosphorus Translocation via Preferential Flow Pathways: A Comparison of Two Sites with Different Phosphorus Stocks. *Front. For. Glob. Change* **2020**, *3*, 48.
54. Kianpoor, K.Y.; Huang, B.; Hu, W.Y. The relation of preferential flow pathways to phosphorus leaching from typical plastic shed vegetable production soils of China. *Agric. Ecosyst. Environ.* **2021**, *307*, 107218. [CrossRef]
55. Kirsten, N.; Grant, M.L.; Macrae, G.A. Differences in preferential flow with antecedent moisture conditions and soil texture: Implications for subsurface P transport. *Hydrol. Process.* **2019**, *33*, 2068–2079.
56. Zhang, W.J.; Jiang, F.Y.; Sun, W.J. Investigating colloid-associated transport of cadmium and lead in a clayey soil under preferential flow conditions. *Water Sci. Technol.* **2021**, *84*, 2486–2498. [CrossRef]
57. Niels, C.; Ginger, B.P.; Parsekian, A.D. Uniform and lateral preferential flows under flood irrigation at field scale. *Hydrol. Process.* **2019**, *33*, 2131–2147.
58. Xue, M.M.; Qing, K.Z.; Lan, M.; Dong, Z.; Yu, W.; Wen, J.H. Effect of stand origin and slope position on infiltration pattern and preferential flow on a Loess hillslope. *Land Degrad. Dev.* **2018**, *29*, 1353–1365.